https://doi.org/10.1016/j.cemconres.2022.106934

Hydration Kinetics and Microstructure Evolution of NaCl-Mixed Tricalcium Silicate Pastes

Yanjie Sun, Jian-xin Lu, Peiliang Shen, Chi Sun Poon*
Department of Civil and Environmental Engineering,
The Hong Kong Polytechnic University, Hung Hom, Kowloon, Hong Kong
Corresponding author email: cecspoon@polyu.edu.hk

Abstract

The hydration of tricalcium silicate (C_3S) pastes mixed with NaCl solutions were investigated at five NaCl concentrations (0 mol/L, 0.029 mol/L, 0.055 mol/L, 0.21 mol/L, and 0.42 mol/L) by performing isothermal calorimetry tests. At the same time, the Boundary Nucleation and Growth (BNG) model was used to analyze the calorimetry data. The model fitted well with the experimental results. C_3S pastes mixed with NaCl solutions followed a similar reaction path to those prepared with DI water, with an accelerated reaction rate as the NaCl concentration increased. The BNG model indicated that the increasing NaCl concentration would significantly increase the nucleation rate of the hydration products, while the hydration product growth rate decreased slightly. The incorporation of NaCl modified the morphology of the early-age calcium silicate hydrates (C-S-H) to relatively shorter and thinner fibers, which resulted in a more compact microstructure and enhanced micromechanical properties than those in pure C_3S pastes.

Keywords: Tricalcium silicate; Sodium Chloride; Nucleation and growth; Microstructure

1. Introduction

In recent years, increasing interest has grown towards research on seawater concrete [1-4]. Most previous studies found that the hydration rate of Portland cement mixed with seawater would be accelerated [2-4]. The early hydration rate of cement profoundly affected the workability of fresh concrete. Thus, the usefulness of seawater concrete depends on controlling the initial reaction rate so that freshly mixed concrete remains fluid and workable before setting. However, seawater and cement were complex systems with various ions and phases, which render thorough study of the hydration process of seawater mixed cement difficult. Chloride is the most abundant element in seawater, where it is mainly present as a sodium salt [5]. Tricalcium silicate (C_3S), known as alite for its impure form, is the dominant phase of anhydrous cement, constituting 50 wt.% - 70 wt.% of the cement mass [6]. The hydration of C_3S is responsible for most of the critical properties of cement and concrete, such as setting, strength, and durability. Therefore, C_3S – NaCl can be used as a model system to study the seawater cement hydration.

In previous studies, it was widely agreed that alkalis accelerated the hydration of cement [7,8] and C_3S [9-12]. The incorporation of NaCl in cement and C_3S mixing led to a shorter induction period and an increased hydration rate at the acceleration hydration period [13,14]. That has been attributed to the fast reactant dissolution [13-15] and hydration product precipitation [15]. Duerden et al. [16] studied the dissolution process of calcium silicate hydrates (C-S-H) and $Ca(OH)_2$ in NaCl solution with NaCl concentrations of less than 1.5 mol/L. The results showed a higher solubility of calcium in NaCl solutions compared with that in DI water. Li et al. [13] indicated that using seawater and NaCl solution in cement mixing would prolong hydration products' nucleation and growth period. Sun et al. [14] studied the reaction of C_3S in NaCl solutions and reported that the dissolution of C_3S was accelerated, and more hydration products were formed than that in the DI water system. Although there were already a few studies on the acceleration phenomenon of C_3S mixed with NaCl solution and seawater, few research has focused on quantifying the kinetics of C_3S pastes mixed with NaCl solutions and establishing the mathematical link with NaCl concentration.

As for the morphology, many studies [12,17-19] reported that the early-age C-S-H grew as fibers in cement and C_3S pastes mixed with DI water. The incorporation of alkali was

reported to modify the morphology of C-S-H fibers [12,18]. The addition of Na_2SO_4 led to divergent needle-like C-S-H fibers, while foil-like C-S-H was formed in C_3S pastes mixed with NaOH solutions. However, it was also reported that NaOH had no apparent effects on C-S-H morphology and composition [20]. As for C-S-H morphology in NaCl-mixed pastes, there was only limited research. Our previous study [14] indicated the fibrillar structure of C-S-H was evident in both DI water and NaCl solution, but no further study was conducted to study the distinction in C_3S pastes with a realistic water to binder ratio (w/b). So, in this study, the C-S-H microstructure evolution in C_3S pastes mixed with NaCl solutions using a range of w/b was studied.

The hydration of C_3S is a complicated process coupling C_3S dissolution, C–S–H and portlandite precipitation [21]. At an early age, the hydration was dominated by nucleation and growth of hydration products, and the precipitation of C-S-H mainly takes place on the surface of C_3S particles [22,23]. Hence, the Boundary Nucleation and Growth (BNG) model was used in this study. BNG model was developed by Thomas [23] via modifying the existing theory pointed out by Cahn [24], applied to phase transformation in a polycrystalline solid. Afterwards, this model was used and verified in many studies on the early hydration of C_3S [25,26] and cement [27]. For example, it was used to study the effects of filler content [28], temperature [29,30], calcium chloride addition [29,31], nanomaterials [32], nucleation seed [33] etc. Based on the BNG model, hydration products' nucleation and growth rates can be quantified. That would help understand the underlying mechanisms for C_3S hydration in NaCl solutions.

This work aimed to investigate the hydration kinetics of C_3S pastes based on the isothermal calorimetry test and the BNG model at five different NaCl concentrations. The morphology evolution and micromechanical properties of hydration products were also characterized to help explain the BNG model results.

2. Materials and methods

2.1 Materials and sample preparation

A laboratory synthesized C_3S was used in this study, prepared with calcium carbonate and silica fume following the procedures developed by Li et al. [34]. The crystalline compositions of the raw material were characterized by X-ray Diffraction (XRD, Rigaku Smartlab, Japan)

with the Rietveld refinement method, and the C_3S purity obtained was 94.1 wt.%. The particle size distribution and specific surface area of the C_3S were measured on the Malvern MS3000 laser particle analyzer, as shown in Fig. 1. The average particle size and specific surface area of the C_3S were 16.9 μm and 7,202 cm^2/g, separately.

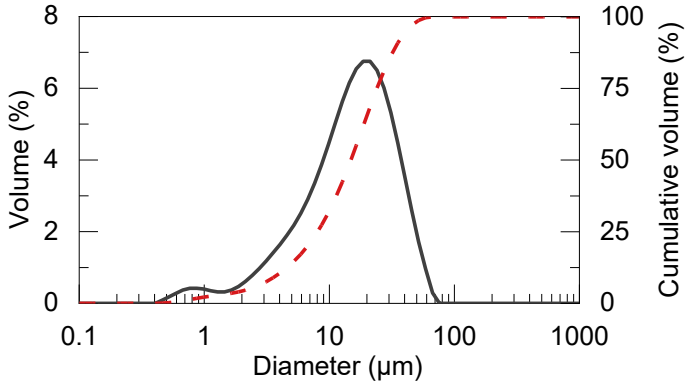

Fig. 1. Particle size distribution of the C_3S.

To investigate the effects of NaCl on C_3S hydration, a series of NaCl solutions were prepared by dissolving an appropriate amount of NaCl reagent (AR-grade) in DI water. The maximum concentration (0.42 mol/L) was consistent with ASTM D1141-98: Standard Practice for the Preparation of Substitute Ocean Water [5]. Besides, 0.21 mol/L, 0.055 mol/L, and 0.029 mol/L of NaCl solutions were also prepared.

2.2 Characterization methods

The hydration kinetics of the C_3S was studied by conducting isothermal calorimetry tests. 10 g C_3S were mixed thoroughly with 5 g of the prepared NaCl solutions and DI water (solution to binder ratio of 0.5), stirred for 1 min by hand in plastic vials before placing the mixtures into the isothermal calorimeter (I-Cal 4000, Calmetrix). Thermal power and energy data were collected under a constant temperature of 20°C for 48 h. -517 J/g was adopted as the enthalpy of ultimate hydration for C_3S to calculate the degree of hydration (DoH), as proposed by Talyor [6].

The morphology evolution of hydration products was observed by scanning electron microscopy (SEM, MAIA3, Tescan) and scanning transmission electron microscopy (STEM

JEM-2100, JEOL). At specified curing times, the hydration of fresh C_3S pastes was stopped by isopropanol before the test.

In order to check the micromechanical properties of early hydration products, C_3S pastes prepared with the same solution/binder ratios were prepared and cured for 24 h and tested by nanoindentation. The tests were conducted on a Nano-indenter (Hysitron TI Premier, Bruker) equipped with a three-sided pyramid Berkovich tip. The surface of the epoxy impregnated C_3S pastes was polished to achieve a smooth surface following the same procedure of a previous study [35]. Before conducting the nanoindentation test, the equipment was calibrated on the standard sample of fused quartz. Fig. 2 shows the loading program and grid arrangement. The maximum loading was 2000 μN reached within 10 s, held for 5 s, and unloaded in 10 s. 10 × 10 testing points with the grid spacing of 10 μm. Three distinct test locations were selected for each specimen.

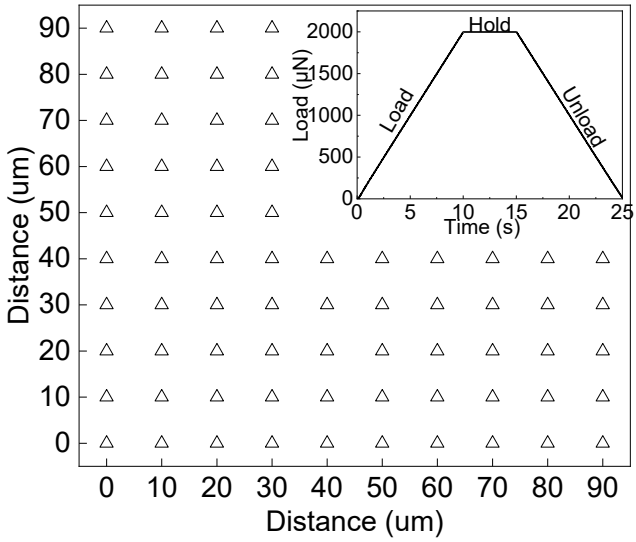

Fig. 2. Loading program and grid arrangement of nanoindentation test.

In order to study the particle contact interactions, a laser particle analyzer (MS3000, Malvern) was employed to follow the particle size evolution of C_3S particles in saturated lime solutions. The solution to binder ratio was chosen as 2000 to meet the requirements of the machine. Suspensions were stirred continuously at a speed of 500 rpm, avoiding the sedimentation of particles. The particle size distribution data were collected every 5 min for

three times. Then, ultrasonic processing was conducted for 30 s at 40 W , followed by the particle size analysis. Ultrasonic activation was able to break the weak contacts between particles due to Van der Waal forces [36,37].

2.3 Boundary nucleation and growth modeling

To study the early hydration kinetics of C_3S pastes, the study focused on the period between the start of water mixing to the point of the deceleration hydration. Experimental observations suggested that the rate of formation of hydration products was the rate-controlling process of C_3S hydration at early ages [22,38]. Thus, models based on nucleation and growth can be used to investigate the early hydration of C_3S. A nucleus is formed after overcoming an energy barrier, and then the hydration products would start to grow as there is a thermodynamic driving force and enough space [39]. The BNG model assumes that particles of the hydration product of C_3S at the early age nucleate on the surface of the C_3S grain. The particles then grow along the boundaries of the C_3S grain at a constant rate. A schematic diagram, as shown in Fig. 3., shows that with a constant growth rate R_g, the cross-sectional circular area A_y between a plane at a distance y and the particle is calculated as Eq. 1.

$$A_y = \pi \left({R_g}^2 (t-\tau)^2 - y^2 \right) \quad (1)$$

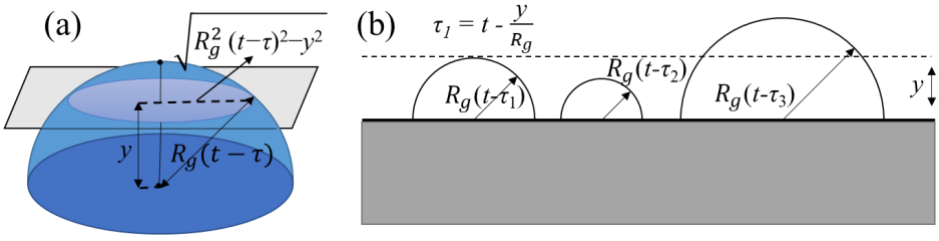

Fig. 3. Schematics of (a) A C_3S hydration product particle nucleated at time τ, the growth rate is R_g, the radius of the particle is $R_g(t-\tau)$, a plane parallel to the boundary at height y intersect with the particle, the radius of the cross-section circle is $\sqrt{{R_g}^2(t-\tau)^2}$. (b) At time t, the intersection between various particles and a plane parallel to the boundary at the distance y, the nucleation time τ should be less than t - y/R_g, so that the particle can reach the plane.

The nucleation rate per unit area of the untransformed boundary is a constant value R_n at an early age, and the total area of the cross-sections between the parallel plane at a distance y and particles denoted A_{tot} can be calculated according to Eq. 2.

$$A_{tot} = \begin{cases} \int_0^{t-\frac{y}{R_g}} R_n \, A_y \, d\tau = \frac{\pi R_n}{3} {R_g}^2 t^3 \left(1 - \frac{3y^2}{{R_g}^2 t^2} + \frac{2y^3}{{R_g}^3 t^3}\right) & t > \frac{y}{R_g} \\ 0 & t < \frac{y}{R_g} \end{cases} \quad (2)$$

Since in the real hydration situation, the hydration product particles would impinge with each other, and the actual total cross-sectional area A_{act} is obtained by modifying Eq.2 to Eq. 3.

$$A_{act} = 1 - \exp\left(-A_{tot}\right) \quad (3)$$

The total volume of particles nucleated on C_3S grain boundaries V_{tot} is the integration of each cross-sectional area from a distance of 0 to $R_g t$, calculated as Eq. 4, where A_b is the boundary area per unit volume.

$$V_{tot} = 2 \int_0^{R_g t} A_b A_{act} \, dy \quad (4)$$

Since the C_3S grain boundaries randomly distribute in the volume, there is a possibility that the impingement of particles nucleated from different boundaries, so the actual volume of hydration product particles V_{act} should be revised as shown in Eq. 5.

$$\begin{aligned} V_{act} &= 1 - \exp(-V_{tot}) \\ &= 1 - \exp\left(-2A_b \int_0^{R_g t} \left(1 - \exp\left(-\frac{\pi R_n}{3} {R_g}^2 t^3 \left(1 - \frac{3y^2}{{R_g}^2 t^2} + \frac{2y^3}{{R_g}^3 t^3}\right)\right)\right) dy\right) \end{aligned} \quad (5)$$

Thus, the actual volume of hydration product particles is dependent on three parameters

A_b, R_n and R_g. These three parameters can be further simplified into two parameters, as shown in Eq. 6 and Eq. 7.

$$k_s = (R_n A_b)^{1/4} {R_g}^{3/4} \quad (6)$$

$$k_p = A_b R_g \quad (7)$$

Where, k_s is an indicator of the rate at which the hydration products cover the surface of C_3S particles while k_p describes the rate at which the hydration products fill the capillary pores between C_3S particles [31]. To fit the isothermal calorimetry data, two more parameters A and t_0, were introduced. A indicates the multiplication factor between heat release and degree of hydration (DoH). The time required for the onset of the nucleation and growth process after mixing is denoted as t_0.

3. Experimental results

3.1 Hydration kinetic analysis

Fig. 4. shows the heat flow and cumulative heat release as a function of time. The data obtained had been normalized to the mass of C_3S. This study defined the ends of the induction and acceleration periods as the inflection points of the heat flow curves. The duration of the induction period decreased from 2.59 h (pure C_3S paste) to 2.11 h (C_3S paste mixed with 0.42 mol/L NaCl solution) due to fast the dissolution of C_3S [40], which was due to the acceleration effect of NaCl solution [14,41]. A higher hydration rate (slope of the heat flow curve) was observed with an increasing NaCl concentration during the acceleration period, indicating a faster formation of hydration products. The peak heat flow value increased to a maximum value (4.61 mW/g) for 0.42 mol/L NaCl, which was more than twice of the control system (2.19 mW/g). The acceleration duration was shortened from 12.00 h to 9.79 h when NaCl concentration was increased from 0 mol/L to 0.42 mol/L. There was an increase in the cumulative heat release of the C_3S mix prepared with NaCl. The effect was more evident with a higher NaCl concentration. The cumulative heat release at 24 h (at which all systems entered the deceleration C3S hydration period) for the C_3S pastes mixed with 0.42 mol/L NaCl, was

the highest with 201.7 J/g. At 48 h, the cumulative heat release increased from 152.7 J/g to 251.1 J/g, as NaCl concentration was increased from 0 mol/L to 0.42 mol/L. These results indicated that more C_3S was hydrated within 48 h in NaCl solutions than in DI water. Moreover, the heat flow after 16 h was similar for all systems, indicating no significant hydration kinetic difference between the different systems after the initial period of hydration.

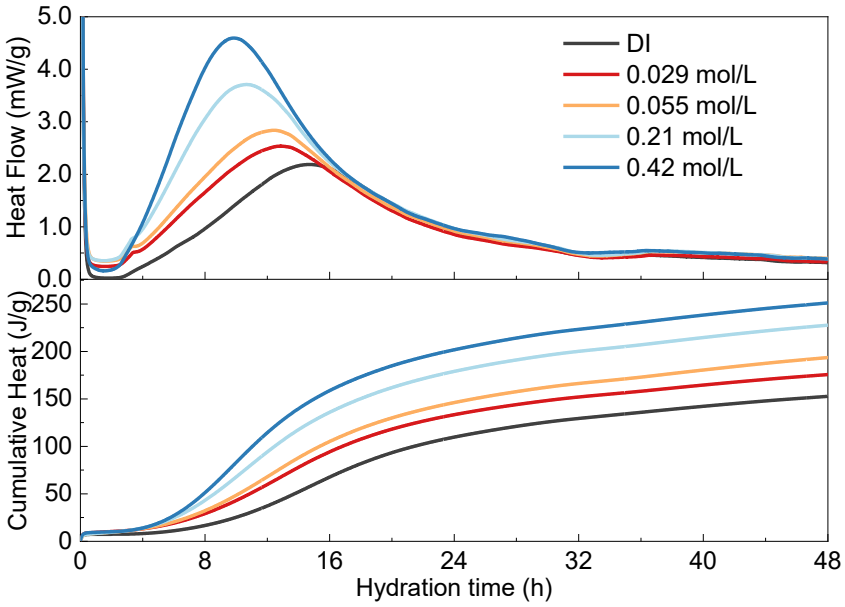

Fig. 4. Influence of NaCl on the hydration heat flow and cumulative heat of C_3S pastes. The concentration of NaCl solutions varied from 0 mol/L to 0.42 mol/L.

Fig. 5. shows the evolution of the heat flow with the increase in DoH. It was also found that with the same DoH, the hydration rate was faster for the NaCl-mixed systems than that prepared with the DI water system. The similar shape of the curves indicated a similar mechanism of hydration. It showed that before the end of the induction period, almost the same amount of C_3S was consumed (about 2%) in all systems, which indicated that the dissolution of C_3S in NaCl solutions was faster than that in DI water. A significant difference was observed when the end of the acceleration period was reached. The heat flow (hydration) rate reached its maximum when the DoH was 11.0% for the control system. As the NaCl concentration increased to 0.42 mol/L, the DoHs for the peak hydration rate increased to 15.5%. With sufficient water, the cause of the end of the acceleration period was due to the space limitation

for the growth of the hydration products , and hence the rate limitation step is diffusion controlled [25,39]. The results thus inferred that the hydration products formed in high NaCl concentration systems were much denser and occupied a smaller volume. That will be further discussed in the following sections.

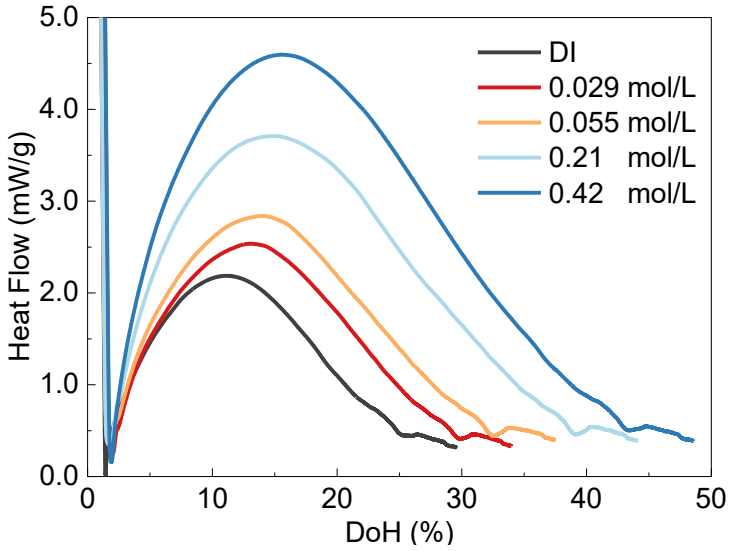

Fig. 5. Influence of varying NaCl concentrations on C_3S hydration.

Effects of the NaCl concentration on the heat release profile were analyzed, as shown in Fig. 6. The NaCl concentration and the time taken to reach the end the induction period were strongly correlated, as shown in Fig. 6a. The intersection of the fitting line was associated with the induction period for pure C_3S pastes. It is affected by various factors, such as the water binder ratio, the particle size of C_3S powder, hydration temperature etc. [23,42,43]. As for the C_3S used in this study, the value was 2.57 h. The function's slope was -1.16, which indicated that increasing NaCl concentration would shorten the induction period linearly, indicating that the dissolution rate of C_3S had a linear relationship with NaCl concentration. Fig. 6b to 6d shows established mathematical functions for the acceleration period duration, the maximum heat flow, and the cumulative heat release. The results indicated that these three values were linearly related to the square root of the NaCl concentration. Similar to the induction period, the intersections for these three functions depended on the intrinsic properties of C_3S and the hydration conditions such as the water binder ratio and hydration temperature. The square root

of NaCl concentration indicated that with the increasing concentration, the effects of NaCl would be reduced gradually. These results indicated that the addition of NaCl contributed to the precipitation of hydration products, but the effect became less obvious as the NaCl concentration increased. The precipitation process was analyzed in more detail with the BNG model in section 3.2, which divided the process into two influence factors, nucleation, and growth.

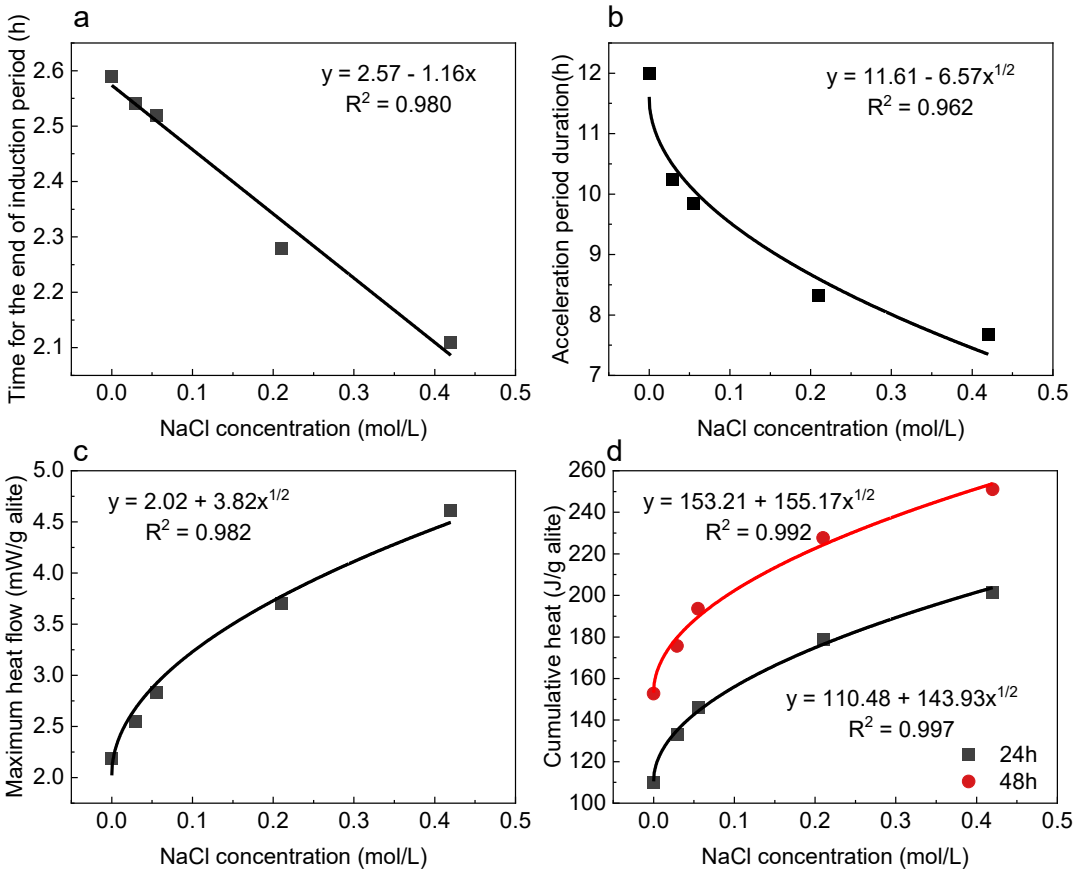

Fig. 6. Influence of NaCl with a varied concentration on (a) end of induction period (b) acceleration period duration (c) heat flow peak value and (d) cumulative heat release for C_3S pastes hydrated for 24 h and 48 h.

3.2 BNG Model analysis

The isothermal calorimetry data were interpreted by applying the BNG model, and the relevant results are shown in Fig. 7. The model fitted the central hydration peak quite well. Deviations were observed particularly at the deceleration periods for all systems. With an

increasing NaCl concentration, the BNG model well fitted the results for higher DoH. The deviation of the modeling from the experimental data was resulted from the change from the nucleation and growth rate control to a diffusion-controlled reaction [31] as the diffusion control process does not follow the assumption of the BNG model [31]. So, the results indicated that the addition of NaCl would delay the impingement of hydrates, probably due to the high packing density of the hydrates.

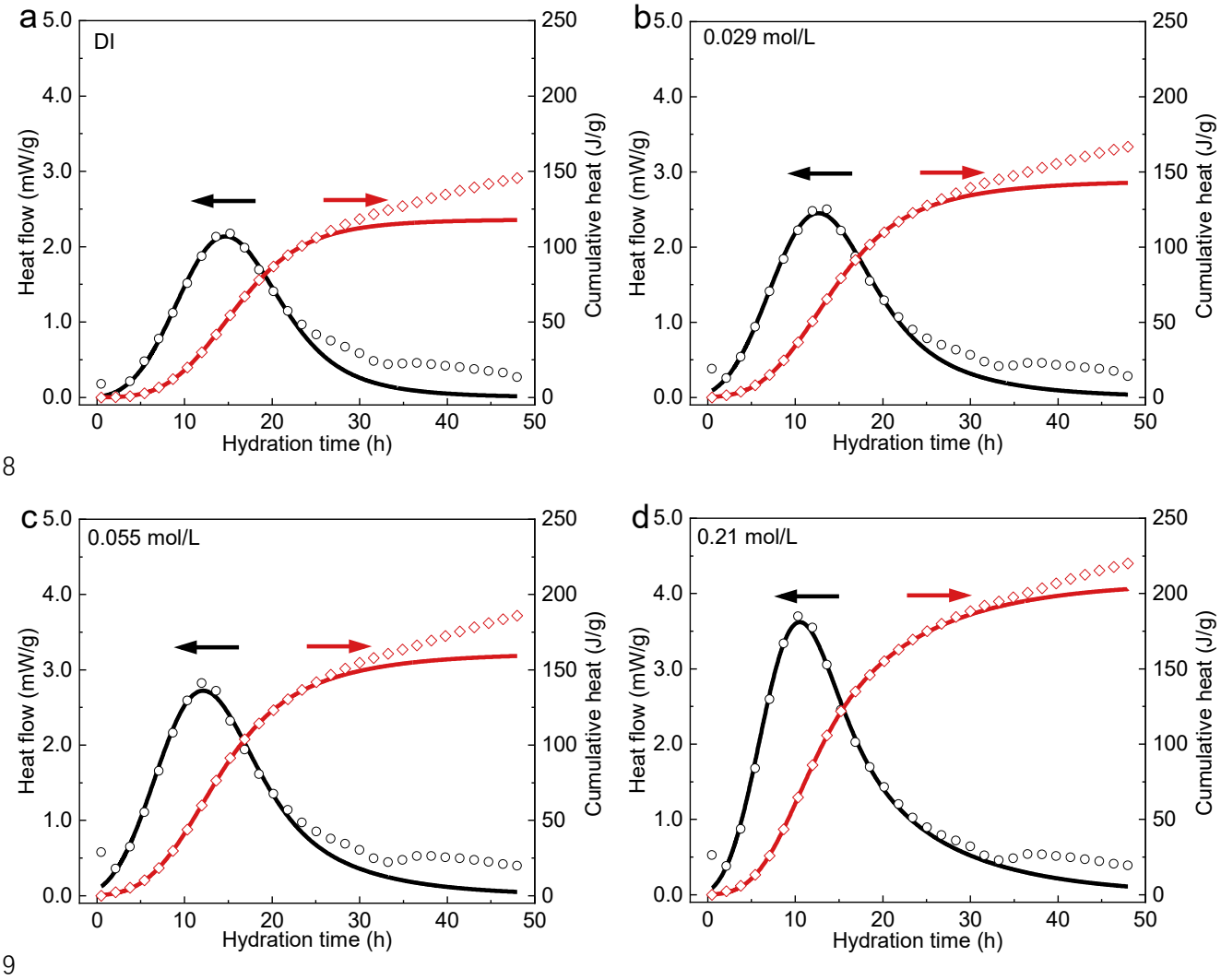

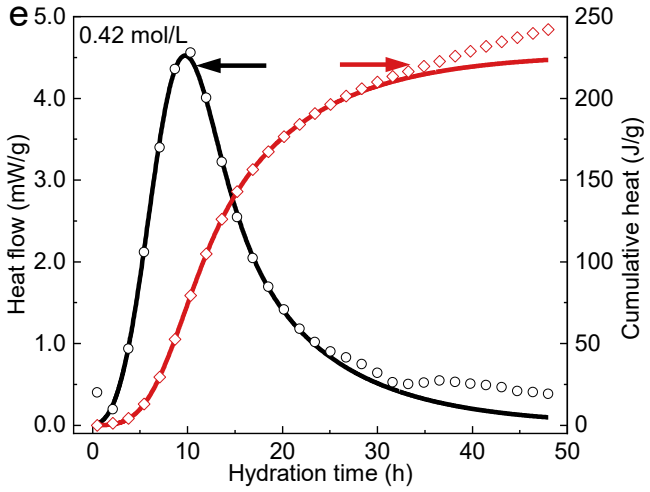

Fig. 7. BNG modelling based on the isothermal calorimetry data for C_3S pastes mixed with (a) DI water (b) 0.029 mol/L NaCl solution (c) 0.055 mol/L NaCl solution (d) 0.21 mol/L NaCl solution and (e) 0.42 mol/L NaCl solution. The open circles and rhombuses are experimental data, and the solid lines are the BNG modeling fits.

The values of the fitting parameters for all systems are given in Table 1. Index A represents the total heat released by the nucleation and growth process. The higher values of A obtained for higher NaCl concentrations thus indicated more hydration products formed in this process. The much smaller A value for the pure C_3S system indicated that the available space for the reaction was occupied at a relatively lower DoH compared with the NaCl-mixed systems. That can be attributed to the lower packing density of the hydrates formed in DI water mixed C_3S pastes. Based on the enthalpy of complete hydration for C_3S, A values corresponded to DoH of about 36% for the control system and about 78% for the system with 0.42 mol/L NaCl. That indicated that for the pure C_3S pastes, the nucleation and growth process dominated only a small fraction of the hydration process, while with the addition of NaCl, the fraction was increased. This result was consistent with the study by Li et al. [13] that the addition of NaCl would extend the nucleation and growth process of hydration products.

Table 1. BNG fitting parameters A_b, t_0, k_s, and k_p for hydration, together with derived physical parameters R_n and R_g.

NaCl concentration (mol/L)	A (J/g)	t_0 (h)	k_s (h^{-1})	k_p (h^{-1})	R_n ($\mu m^{-2} h^{-1}$)	R_g ($\mu m\ h^{-1}$)
0	118 (2)	-1.74 (3)	0.055 (5)	0.066 (4)	0.038 (4)	0.060 (4)
0.029	144 (2)	-3.35 (3)	0.056 (5)	0.051 (4)	0.084 (4)	0.047 (4)
0.055	160 (2)	-3.46 (3)	0.057 (5)	0.049 (4)	0.109 (4)	0.044 (4)
0.21	207 (2)	-2.05 (3)	0.068 (5)	0.040 (4)	0.394 (4)	0.037 (4)
0.42	227 (2)	-0.66 (4)	0.082 (5)	0.044 (5)	0.625 (5)	0.040 (5)

The time constant t_0 was negative. It may be attributed to the prior formation of C-S-H nuclei before mixing. For the NaCl-mixed systems, the t_0 values were more negative, indicating NaCl accelerated the very early hydration before the acceleration period. That was consistent with our previous research that NaCl contributed to the dissolution of C_3S [14].

The surface area parameter, A_b, can be calculated via dividing the specific surface area of C_3S powder (7202 cm^2/g) by the volume occupied of the hydration products after complete hydration, based on the hydration process as shown in Eq. 8. The density of C-S-H and $Ca(OH)_2$ were approximately 2.1 g/cm^3 and 2.24 g/cm^3 [23], respectively. Therefore, the complete hydration volume of C_3S was calculated to be 0.6628 cm^3/g. That gave the A_b = 1.09 μm^{-1}. The resulting growth rates and nucleation rates calculated from Eq. 6 and Eq. 7 are also given in Table 1.

$$3CaO \cdot SiO_2 + 5.3H_2O \rightarrow 1.7CaO\text{-}SiO_2\text{-}4H_2O + 1.3Ca(OH)_2 \quad (8)$$

It shows that the values of nucleation rate constant R_n was over 16 times as high in the 0.42 mol/L NaCl system as in the control system, while the values of growth rate constant R_g decreased with the addition of NaCl, but the deviation was not as significant as that of R_n. These results indicated that incorporating NaCl in C_3S paste mixing would accelerate the nuclei formation on the surface but retard the growth of hydrates.

3.3 Morphology of hydration products

To help understand the influence of NaCl on the nucleation and growth of hydrates. SEM and STEM images were acquired at various curing times. In the SEM images, as shown by Fig. 8. At 5 min, this was in the dissolution process, and the smooth surfaces were observed for all systems. At 1st h, and during the induction period for all pastes, a few nuclei were observed, and the number of nuclei for NaCl mixed systems was higher than that of the pure C_3S system. By the end of the induction period (2.59 h for the DI system and 2.11 h for 0.42 mol/L NaCl system), a significant amount of nuclei were found on the surface of C_3S. However, no significant distinction was found. The apparent difference can be observed at 4th h, where both systems were in their acceleration period. For the DI system, the number of nuclei did not increase much compared with that at 2.59 h, but the nuclei grew bigger compared with those in the NaCl system. For NaCl mixed system, the surface of C_3S was covered with more small nuclei. These results were consistent with the BNG modeling results that with the incorporation of NaCl, the nucleation rate of hydrates increased, but the growth of hydration products was retarded.

The STEM images from 5 min to 4 h are also shown in Fig. 9. Similar to the SEM observation, at 5th min, there was only dissolution happening, so there were no nuclei on the surface. From 1st h to the end of the induction period. The nuclei steadily appeared on the surface of C_3S. At 4th h, a clear difference in C-S-H length and thickness between the pure C_3S and the NaCl mixed pastes. For the pure C_3S pastes, the C-S-H fibers tended to form thicker and longer structures. For NaCl mixed system, the STEM characterization showed that the C–S–H morphology was modified to thinner and shorter fibers. The addition of NaCl increased the calcium concentration in the solution during the early hydration period [14], which was likely to affect the formation of hydrates. Gaboriaud et al. [44] indicated that relatively large particles were formed at low calcium concentrations. In contrast, smaller aggregations were formed rapidly at a high calcium concentration. That was in good agreement with the STEM results for the first several hours of hydration. Alkali was uptaken by the gel products [45-51] which resulted in the formation of shorter average chain length C-S-H [49,52,53]. That could be another reason for the short fiber formation.

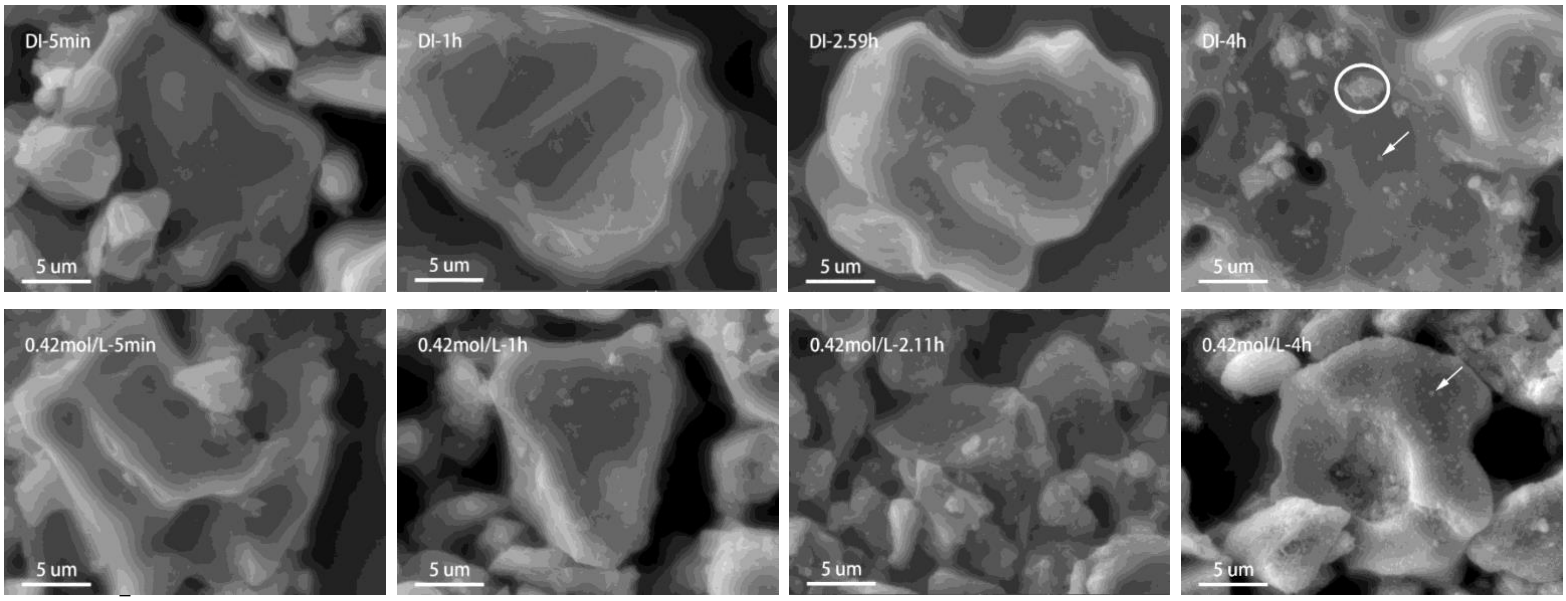

Fig. 8. SEM images of microstructure evolution via time. Small nuclei were observed as indicated by arrows. For pure C_3S pastes, large clusters of hydration products were also observed at 4 h, indicated by the circle

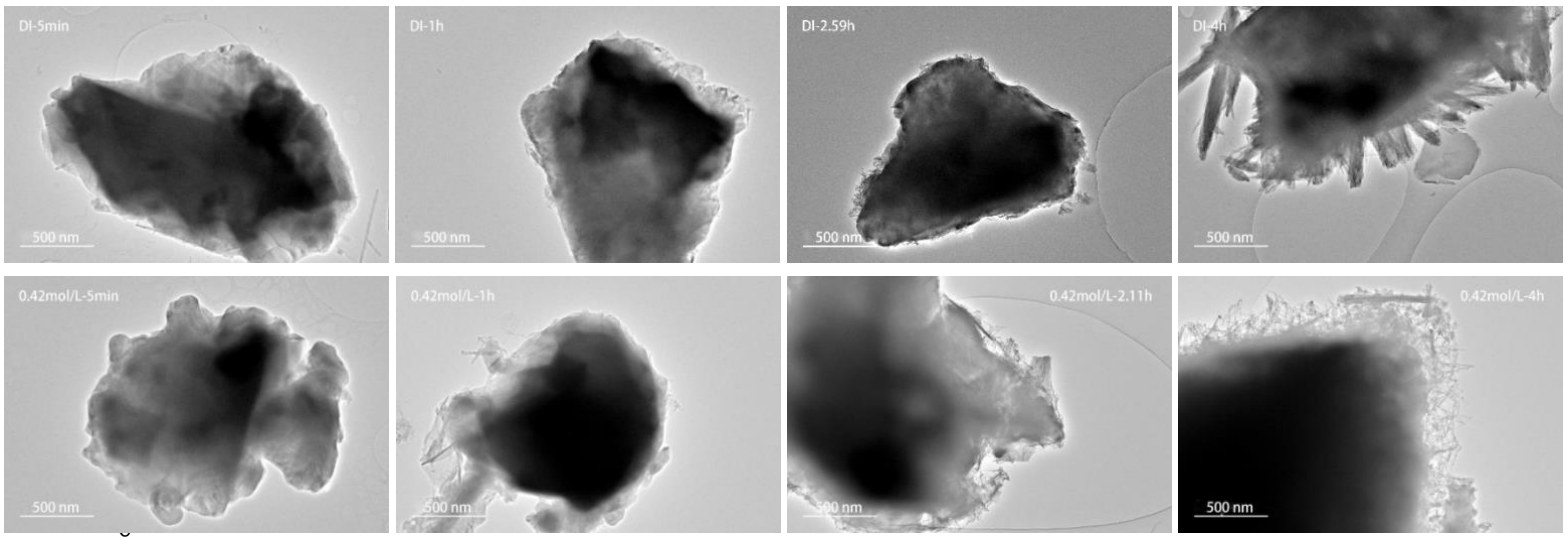

Fig. 9. STEM images of microstructure evolution via time

3.4 Nanoindentation analysis

Nanoindentation test was conducted for the hydrated C_3S pastes cured for 24 h. The pastes were already set and still in the BNG controlling period as indicated in section 3.2. The nanoindentation test was analyzed by cluster analysis as in a previous research [35], as shown in Fig. 10. The data were divided into four phases (low density (LD) C-S-H, high density (HD)

C-S-H, portlandite, and C_3S) as suggested by Hu et al. [54].

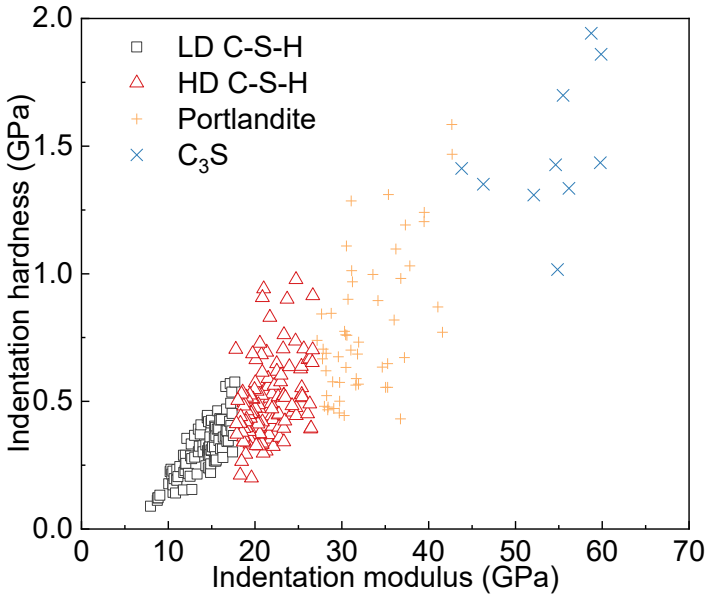

Fig. 10. Cluster analysis for pure C_3S pastes curing for 24 h. Irregular curves were eliminated before analysis, and four phases were divided from the overall data.

Based on the multivariate cluster analysis results, the average indentation modulus and hardness were calculated and presented in Fig. 11. It showed that the micromechanical properties of C-S-H were improved with the addition of NaCl. For indentation modulus of LD C-S-H, the value for C_3S pastes prepared with 0.42 mol/L NaCl was 15.62 ± 2.13 GPa, while the value for the pastes mixed with DI water only was 14.27 ± 1.57 GPa. The indentation modulus of HD C-S-H was also enhanced with the addition of NaCl. For indentation hardness of LD C-S-H, the value was increased from 0.39 ± 0.08 GPa to 0.51 ± 0.15 GPa with the incorporation of NaCl. C_3S pastes mixed with 0.42 mol/L NaCl also produced HD C-S-H with a higher indentation hardness compared with the pure C_3S pastes. The micromechanical properties of C-S-H should have a positive relationship with the packing density [55]. Thus, we can infer that the early-age C-S-H formed in NaCl-mixed C_3S pastes had a higher packing density. The results were consistent with the BNG modeling that it needed a higher DoH to reach the diffusion control process in NaCl systems. Mendoza et al. [56] reported a similar result that incorporating alkali cations would increase the elastic modulus of C-S-H due to the

electrostatic attraction between cations (positively charged) and C-S-H (negatively charged).

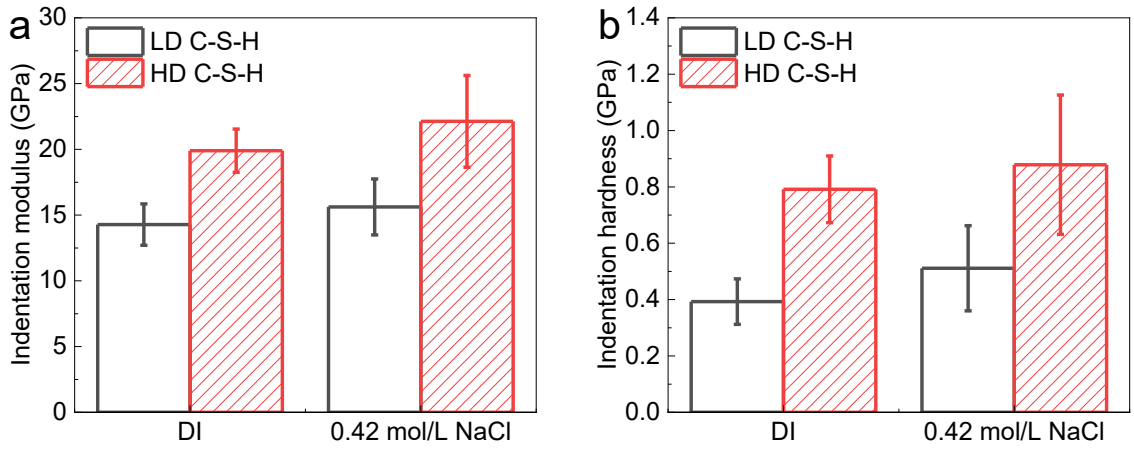

Fig. 11. Cluster analysis results for (a) indentation modulus and (b) indentation hardness for C_3S pastes mixed with DI water and 0.42mol/L NaCl

3.5 Coagulation and rigidification

The setting of C_3S pastes would normally take place in two steps: coagulation and rigidification [38]. To study the effects of NaCl on the setting behavior of C_3S at an early age, a granulometric method as proposed by Jiang et al. [36,37] was used to measure the mean particle size of the C_3S particle evolution in diluted suspensions (have you described the method w/b). The study would help understand the surface contact interactions between the particles. The aggregates were taken as a single particle, and the results are shown in Fig. 12. For better visualization, the details were amplified as inserts in each figure. Agglomeration was mainly attributed to Van der Waals forces at an early age [36,37], so the ultrasonic processing could break part of the agglomerations, producing a dispersed suspension. As the hydration progressed, more and more strong interactions formed among particles, e.g., crystalline bonding. Then the ultrasonic force could not break the large particles, resulting in rigidification. The coagulation and rigidification processes were clearly distinguished by whether the particles could be broken after the ultrasonic processing. The time for rigidification was also clearly determined based on the results, which were 109 min and 73min for the DI water and 0.42 mol/L NaCl systems, respectively. It was consistent with the kinetic analysis above which indicated that the incorporation of NaCl accelerated the hydration of C_3S. The rigidification

process was also accelerated with the addition of NaCl. That was because the hydrate formation was accelerated due to the increase of the number of nuclei, as mentioned in section 3.2 and section 3.3.

There was another interesting result observed from the particle size evolution. After rigidification, the particle size for 0.42 mol/L NaCl solution suspension was significantly larger than that of the DI water suspension, resulting in a smaller specific area. That was consistent with BNG modeling and nanoindentation test results that incorporating NaCl increased the packing density of C-S-H formed at the early age, so the same amount of hydrates occupied a relatively smaller space compared with that in the DI water system. That retarded the impingement of hydrates, and the nucleation and growth process thus dominated for a more extended period.

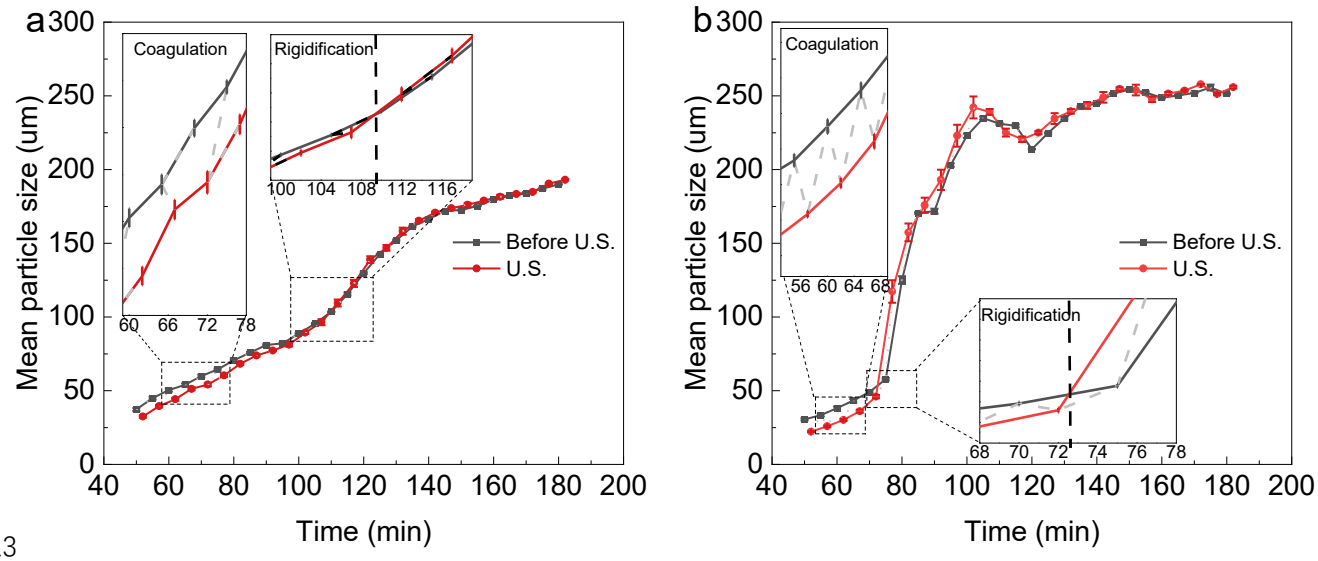

Fig. 12. Evolution of mean particle size in C_3S suspensions for (a) DI water and (b) 0.42 mol/L NaCl solution. U.S. represented ultrasonic processing. In the beginning, the coagulation was mainly due to Van der Waals forces, while for the rigidification process, the crystalline bonding dominated, so the ultrasonic process could not break the structure.

4. Discussion

This work aimed to provide a deeper insight into the hydration kinetics of C_3S pastes prepared by mixing with NaCl solutions. It was found that the induction period decreased as

the NaCl concentration increased, and they were linearly correlated. The mechanism of the occurrence of the induction period has been a controversial subject. There are mainly two possible mechanisms proposed, namely (i) the metastable barrier hypothesis [57] and (ii) the geochemical dissolution theory [58,59]. However, both theories agreed that the dissolution of C_3S and the number of nuclei formed were the dominant factors [38,40]. Our previous work [14] had reported that NaCl would accelerate the dissolution of C_3S. The increase of NaCl concentration improved the ionic strength of the pore solutions, and consequently decreased the activity coefficients of calcium, silicate, and hydroxide ions. That contributed to the deviation of the solubility equilibrium and a faster dissolution of C_3S [41]. Combined with the results of this study, we also found that the nucleation rate of was accelerated in the NaCl solutions. This can be another reason for the shortened induction period, which was resulted from the high calcium concentration [38].

The nucleation and growth process showed a distinctive difference between the C_3S pastes mixed with DI water and NaCl solution. Based on the calorimetry test and BNG modeling, it was found that the hydration of C_3S was accelerated with the addition of NaCl, which was similar to the findings of many previous studies [13,14]. With the increase of NaCl concentration, this accelerating effect became more pronounced. The BNG modeling results indicated that the addition of NaCl would increase the nucleation rate of hydrates significantly while the growth rate was decreased slightly. That was consistent with our previous study [14] that adding NaCl would increase the calcium concentration in the pore solution. The high calcium concentration contributed to the nucleation of the hydrates. It was also found that the BNG dominated the hydration for a higher DoH in the NaCl-mixed system. Since there was sufficient water for C_3S hydration, the end of the BNG process would start due to space limitation, and then diffusion control started to dominate [25,39]. Thus, it was deduced that at the same DoH, the C-S-H formed in NaCl-mixed pastes occupied less space than in the reference system (i.e. the packing density of the early-age C-S-H was increased with the incorporation of NaCl). This deduction was verified by the nanoindentation test and particle size analysis. Similar results had been reported that the incorporation of alkalis reduced the specific area hydration products [12,60], which was attributed to the electrostatic attraction

between the alkali cations and C-S-H particles [56].

Another interesting result was the difference in morphologies of C-S-H formed in DI water and NaCl solution. Based on the SEM and STEM observations, a schematic illustration is shown as in Fig. 13. The C-S-H formed in DI water was long and thick fibers, but the number of nuclei was relatively fewer than that in NaCl solution. As hydration progressed, the C-S-H fibers could impinge on other particles, halting further growth. Due to space limitation, the dominating reaction process changed to be diffusion control [25]. Unlike the C_3S hydrated with DI water, the C-S-H fibers formed in NaCl solutions were shorter and thinner. The electrostatic attraction caused a denser packing of hydrates, and the impingement of hydration products was retarded. Thus, the hydration rate of NaCl-mixed mixed systems was at a higher value at the same DoH as indicated by Fig. 5.

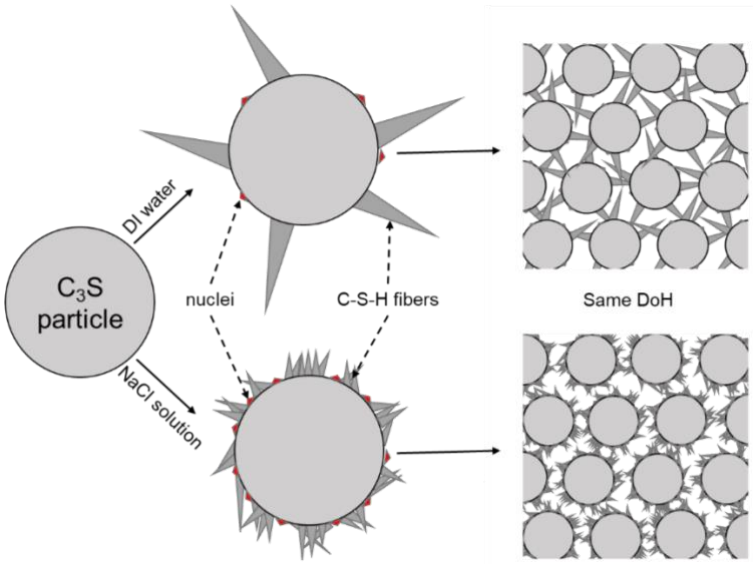

Fig. 13. Schematic for hydrates nucleation and growth in DI water and NaCl solution.

5. Conclusions

C_3S was mixed with DI water and NaCl solutions with varying concentrations to study the hydration kinetics and microstucture evolution. Based on the results, the following conclusions can be drawn:

- The incorporation of NaCl accelerated the hydration of C_3S. With the increase of NaCl concentration (within 0.42 mol/L), the acceleration effect was more

pronounced.

- The nucleation rate of hydrates increased obviously in NaCl solutions, and a higher rate was recorded with a high NaCl concentration. In contrast, the growth rate decreased slightly with the NaCl solutions.
- The C-S-H formed within the C_3S pastes mixed with DI water were long and thick fibers, while the C-S-H formed in the NaCl-mixed pastes were short and thin fibers. The micromechanical properties of C-S-H formed in the NaCl-mixed pastes were improved as compared to those in the pure C_3S pastes.

Acknowledgment

The work described in this paper was supported by the Theme-Based Research Scheme of the Research Grants Council of the Hong Kong SAR Government (Project No. T22-502/18-R).

References

[1] M. Guo, B. Hu, F. Xing, X. Zhou, M. Sun, L. Sui, Y. Zhou, Characterization of the mechanical properties of eco-friendly concrete made with untreated sea sand and seawater based on statistical analysis, Constr. Build. Mater. 234 (2020) 117339. https://doi.org/10.1016/j.conbuildmat.2019.117339.

[2] J. Wang, E. Liu, L. Li, Multiscale investigations on hydration mechanisms in seawater OPC paste, Constr. Build. Mater. 191 (2018) 891-903. https://doi.org/10.1016/j.conbuildmat.2018.10.010.

[3] J. Xiao, C. Qiang, A. Nanni, K. Zhang, Use of sea-sand and seawater in concrete construction: Current status and future opportunities, Constr. Build. Mater. 155 (2017) 1101-1111. https://doi.org/10.1016/j.conbuildmat.2017.08.130.

[4] A. Younis, U. Ebead, P. Suraneni, A. Nanni, Fresh and hardened properties of seawater-mixed concrete, Constr. Build. Mater. 190 (2018) 276-286. https://doi.org/10.1016/j.conbuildmat.2018.09.126.

[5] ASTM D1141-98(2013), Standard practice for the preparation of substitute ocean water, ASTM International, West Conshohocken, PA, 2013, www.astm.org

[6] H.F. Taylor, Cement chemistry, second ed., Thomas Telford, London, 1997.

[7] X. Zhou, X. Lin, M. Huo, Y. Zhang, The hydration of saline oil-well cement, Cem. Concr. Res. 26(12) (1996) 1753-1759. https://doi.org/10.1016/S0008-8846(96)00176-7.

[8] C.A.A. Rocha, G.C. Cordeiro, R.D. Toledo Filho, Use of thermal analysis to determine the hydration products of oil well cement pastes containing NaCl and KCl, J. Therm. Anal. Calorim. 122(3) (2015) 1279-1288. https://doi.org/10.1007/s10973-015-4949-6.

[9] J.J. Thomas, H.M. Jennings, Free-Energy-Based Model of Chemical Equilibria in the CaO–SiO_2-H_2O System, J. Am. Ceram. Soc. 81(3) (1998) 606-612. https://doi.org/10.1111/j.1151-

2916.1998.tb02380.x.
[10] D.E. Macphee, K. Luke, F.P. Glasser, E.E. Lachowski, Solubility and aging of calcium silicate hydrates in alkaline solutions at 25°C, J. Am. Ceram. Soc. 72(4) (1989) 646-654. https://doi.org/10.1111/j.1151-2916.1989.tb06189.x.
[11] D.L. Kantro, Tricalcium silicate hydration in the presence of various salts, J. Test. Eval. 3(4) (1975) 312-321. https://doi.org/10.1520/JTE10661J.
[12] B. Mota, T. Matschei, K. Scrivener, The influence of sodium salts and gypsum on alite hydration, Cem. Concr. Res. 75 (2015) 53-65. https://doi.org/10.1016/j.cemconres.2015.04.015.
[13] W. Li, Z. Jiang, M. Lu, W. Long, F. Xing, J. Liu, Effects of seawater, NaCl, and Na_2SO_4 solution mixing on hydration process of cement paste, J. Mater. Civ. Eng. 33(5) (2021) 04021057. https://doi.org/10.1061/(ASCE)MT.1943-5533.0003673.
[14] Y. Sun, Y. Zhang, Y. Cai, W.L. Lam, J.-X. Lu, P. Shen, C.S. Poon, Mechanisms on accelerating hydration of alite mixed with inorganic salts in seawater and characteristics of hydration products, ACS Sustain. Chem. Eng. 9(31) (2021) 10479-10490. https://doi.org/10.1021/acssuschemeng.1c01730.
[15] J.F. Young, H.S. Tong, R.L. Berger, Compositions of solutions in contact with hydrating tricalcium silicate pastes, J. Am. Ceram. Soc. 60(5-6) (1977) 193-198. https://doi.org/10.1111/j.1151-2916.1977.tb14104.x.
[16] S. Duerden, F.P. Glasser, K. Goldthorpe, J. Pedersen, K. Quillin, D. Ross, S.A. Stronach, M. Tyrer, Chemistry and performance of blended cements and backfills for use in radioactive waste disposal, Mater. Res. Soc. Symp. Proc. 465(1) (1996) 287-294. https://doi.org/10.1557/PROC-465-287.
[17] I.G. Richardson, Tobermorite/jennite- and tobermorite/calcium hydroxide-based models for the structure of C-S-H: applicability to hardened pastes of tricalcium silicate, β-dicalcium silicate, Portland cement, and blends of Portland cement with blast-furnace slag, metakaolin, or silica fume, Cem. Concr. Res. 34(9) (2004) 1733-1777. https://doi.org/10.1016/j.cemconres.2004.05.034.
[18] B. Mota, T. Matschei, K. Scrivener, Impact of NaOH and Na_2SO_4 on the kinetics and microstructural development of white cement hydration, Cem. Concr. Res. 108 (2018) 172-185. https://doi.org/10.1016/j.cemconres.2018.03.017.
[19] L. Nguyen-Tuan, M.A. Etzold, C. Rößler, H.-M. Ludwig, Growth and porosity of C-S-H phases using the sheet growth model, Cem. Concr. Res. 129 (2020) 105960. https://doi.org/10.1016/j.cemconres.2019.105960.
[20] A. Kumar, G. Sant, C. Patapy, C. Gianocca, K.L. Scrivener, The influence of sodium and potassium hydroxide on alite hydration: Experiments and simulations, Cem. Concr. Res. 42(11) (2012) 1513-1523. https://doi.org/10.1016/j.cemconres.2012.07.003.
[21] L. Nicoleau, A. Nonat, A new view on the kinetics of tricalcium silicate hydration, Cem. Concr. Res. 86 (2016) 1-11. https://doi.org/10.1016/j.cemconres.2016.04.009.
[22] S. Garrault, A. Nonat, Hydrated layer formation on tricalcium and dicalcium silicate surfaces: experimental study and numerical simulations, Langmuir 17(26) (2001) 8131-8138. https://doi.org/10.1021/la011201z.
[23] J.J. Thomas, A new approach to modeling the nucleation and growth kinetics of tricalcium silicate hydration, J. Am. Ceram. Soc. 90(10) (2007) 3282-3288.

https://doi.org/10.1111/j.1551-2916.2007.01858.x.
[24] J.W. Cahn, The kinetics of grain boundary nucleated reactions, Acta Metall. 4(5) (1956) 449-459. https://doi.org/10.1016/0001-6160(56)90041-4.
[25] S. Bishnoi, K.L. Scrivener, Studying nucleation and growth kinetics of alite hydration using μic, Cem. Concr. Res. 39(10) (2009) 849-860. https://doi.org/10.1016/j.cemconres.2009.07.004.
[26] Z. Zhang, F. Han, P. Yan, Modelling the dissolution and precipitation process of the early hydration of C_3S, Cem. Concr. Res. 136 (2020) https://doi.org/10.1016/j.cemconres.2020.106174.
[27] G.W. Scherer, J. Zhang, J.J. Thomas, Nucleation and growth models for hydration of cement, Cem. Concr. Res. 42(7) (2012) 982-993. https://doi.org/10.1016/j.cemconres.2012.03.019.
[28] T. Oey, A. Kumar, J.W. Bullard, N. Neithalath, G. Sant, The filler effect: The influence of filler content and surface area on cementitious reaction rates, J. Am. Ceram. Soc. 96(6) (2013) 1978-1990. https://doi.org/10.1111/jace.12264.
[29] J. Zhang, E.A. Weissinger, S. Peethamparan, G.W. Scherer, Early hydration and setting of oil well cement, Cem. Concr. Res. 40(7) (2010) 1023-1033. https://doi.org/10.1016/j.cemconres.2010.03.014.
[30] Z. Zhang, P. Yan, Hydration kinetics of the epoxy resin-modified cement at different temperatures, Constr. Build. Mater. 150 (2017) 287-294. https://doi.org/10.1016/j.conbuildmat.2017.05.225.
[31] J.J. Thomas, A.J. Allen, H.M. Jennings, Hydration kinetics and microstructure development of normal and $CaCl_2$-accelerated tricalcium silicate pastes, J. Phys. Chem. C. 113(46) (2009) 19836-19844. https://doi.org/10.1021/jp907078u.
[32] B.Y. Lee, K.E. Kurtis, Influence of TiO_2 Nanoparticles on Early C_3S Hydration, J. Am. Ceram. Soc. 93(10) (2010) 3399-3405. https://doi.org/10.1111/j.1551-2916.2010.03868.x.
[33] G.W. Scherer, F. Bellmann, Kinetic analysis of C-S-H growth on calcite, Cem. Concr. Res. 103 (2018) 226-235. https://doi.org/10.1016/j.cemconres.2016.07.017.
[34] X.R. Li, A. Ouzia, K. Scrivener, Laboratory synthesis of C_3S on the kilogram scale, Cem. Concr. Res. 108 (2018) 201-207. https://doi.org/10.1016/j.cemconres.2018.03.019.
[35] Y. Sun, J.-X. Lu, C.S. Poon, Strength degradation of seawater-mixed alite pastes: an explanation from statistical nanoindentation perspective, Cem. Concr. Res. 152 (2022) 106669. https://doi.org/10.1016/j.cemconres.2021.106669.
[36] S.P. Jiang, J.C. Mutin, A. Nonat, Studies on mechanism and physico-chemical parameters at the origin of the cement setting II. Physico-chemical parameters determining the coagulation process, Cem. Concr. Res. 26(3) (1996) 491-500. https://doi.org/10.1016/S0008-8846(96)85036-8.
[37] S.P. Jiang, J.C. Mutin, A. Nonat, Studies on mechanism and physico-chemical parameters at the origin of the cement setting. I. The fundamental processes involved during the cement setting, Cem. Concr. Res. 25(4) (1995) 779-789. https://doi.org/10.1016/0008-8846(95)00068-N.
[38] S. Garrault-Gauffinet, A. Nonat, Experimental investigation of calcium silicate hydrate (CSH) nucleation, J. Cryst. Growth. 200(3-4) (1999) 565-574. https://doi.org/10.1016/S0022-0248(99)00051-2.

[39] J.J. Thomas, J.J. Biernacki, J.W. Bullard, S. Bishnoi, J.S. Dolado, G.W. Scherer, A. Luttge, Modeling and simulation of cement hydration kinetics and microstructure development, Cem. Concr. Res. 41(12) (2011) 1257-1278. https://doi.org/10.1016/j.cemconres.2010.10.004.
[40] P. Juilland, A. Kumar, E. Gallucci, R.J. Flatt, K.L. Scrivener, Effect of mixing on the early hydration of alite and OPC systems, Cem. Concr. Res. 42(9) (2012) 1175-1188. https://doi.org/10.1016/j.cemconres.2011.06.011.
[41] L. Nicoleau, E. Schreiner, A. Nonat, Ion-specific effects influencing the dissolution of tricalcium silicate, Cem. Concr. Res. 59 (2014) 118-138. https://doi.org/10.1016/j.cemconres.2014.02.006.
[42] J.J. Thomas, H.M. Jennings, Effects of D_2O and mixing on the early hydration kinetics of tricalcium silicate, Chem. Mater. 11(7) (1999) 1907-1914. https://doi.org/10.1021/cm9900857.
[43] S. Garrault, T. Behr, A. Nonat, Formation of the C−S−H layer during early hydration of tricalcium silicate grains with different sizes, J. Phys. Chem. B. 110(1) (2006) 270-275. https://doi.org/10.1021/jp0547212.
[44] F. Gaboriaud, A. Nonat, D. Chaumont, A. Craievich, Aggregation processes and formation of silico-calco-alkaline gels under high ionic strength, J. Colloid Interface Sci. 253(1) (2002) 140-9. https://doi.org/10.1006/jcis.2002.8522.
[45] S.-Y. Hong, F.P. Glasser, Alkali binding in cement pastes: Part I. The C-S-H phase, Cem. Concr. Res. 29(12) (1999) 1893-1903. https://doi.org/10.1016/S0008-8846(99)00187-8.
[46] A. Leemann, L. Lörtscher, L. Bernard, G. Le Saout, B. Lothenbach, R.M. Espinosa-Marzal, Mitigation of ASR by the use of $LiNO_3$—Characterization of the reaction products, Cem. Concr. Res. 59 (2014) 73-86. https://doi.org/10.1016/j.cemconres.2014.02.003.
[47] H. Stade, On the reaction of C-S-H(di, poly) with alkali hydroxides, Cem. Concr. Res. 19(5) (1989) 802-810. https://doi.org/10.1016/0008-8846(89)90051-3.
[48] H. Viallis, P. Faucon, J. Petit, A. Nonat, Interaction between salts (NaCl, CsCl) and calcium silicate hydrates (C−S−H), J. Phys. Chem. B. 103(25) (1999) 5212-5219. https://doi.org/10.1021/jp983757+.
[49] E. L'Hopital, B. Lothenbach, G. Le Saout, D. Kulik, K. Scrivener, Incorporation of aluminium in calcium-silicate-hydrates, Cem. Concr. Res. 75 (2015) 91-103. https://doi.org/10.1016/j.cemconres.2015.04.007.
[50] T. Missana, M. García-Gutiérrez, M. Mingarro, U. Alonso, Comparison between cesium and sodium retention on calcium silicate hydrate (CSH) phases, Appl. Geochem. 98 (2018) 36-44. https://doi.org/10.1016/j.apgeochem.2018.09.007.
[51] T.T.H. Bach, E. Chabas, I. Pochard, C. Cau Dit Coumes, J. Haas, F. Frizon, A. Nonat, Retention of alkali ions by hydrated low-pH cements: Mechanism and Na^+/K^+ selectivity, Cem. Concr. Res. 51 (2013) 14-21. https://doi.org/10.1016/j.cemconres.2013.04.010.
[52] B. Lothenbach, A. Nonat, Calcium silicate hydrates: Solid and liquid phase composition, Cem. Concr. Res. 78 (2015) 57-70. https://doi.org/10.1016/j.cemconres.2015.03.019.
[53] S. Yoon, J. Ha, S.R. Chae, D.A. Kilcoyne, P.J.M. Monteiro, X-ray spectromicroscopic study of interactions between NaCl and calcium silicate hydrates, Mag. Concr. Res. 66(3) (2014) 141-149. https://doi.org/10.1680/macr.13.00244.
[54] C. Hu, Z. Li, Micromechanical investigation of Portland cement paste, Constr. Build. Mater. 71 (2014) 44-52. https://doi.org/10.1016/j.conbuildmat.2014.08.017.
[55] M. Vandamme, F.-J. Ulm, P. Fonollosa, Nanogranular packing of C–S–H at

substochiometric conditions, Cem. Concr. Res. 40(1) (2010) 14-26. https://doi.org/10.1016/j.cemconres.2009.09.017.
[56] O. Mendoza, C. Giraldo, S.S. Camargo, J.I. Tobón, Structural and nano-mechanical properties of Calcium Silicate Hydrate (C-S-H) formed from alite hydration in the presence of sodium and potassium hydroxide, Cem. Concr. Res. 74 (2015) 88-94. https://doi.org/10.1016/j.cemconres.2015.04.006.
[57] H. Jennings, P. Pratt, An experimental argument for the existence of a protective membrane surrounding Portland cement during the induction period, Cem. Concr. Res. 9(4) (1979) 501-506. https://doi.org/10.1016/0008-8846(79)90048-6.
[58] P. Barret, D. Ménétrier, D. Bertrandie, Mechanism of C_3S dissolution and problem of the congruency in the very initial period and later on, Cem. Concr. Res. 13(5) (1983) 728-738. https://doi.org/10.1016/0008-8846(83)90064-9.
[59] S. Garrault, E. Finot, E. Lesniewska, A. Nonat, Study of CSH growth on C_3S surface during its early hydration, Mater. Struct. 38(4) (2005) 435-442. https://doi.org/10.1007/BF02482139.
[60] I. Jawed, J. Skalny, Alkalies in cement: A review: II. Effects of alkalies on hydration and performance of Portland cement, Cem. Concr. Res. 8(1) (1978) 37-51. https://doi.org/10.1016/0008-8846(78)90056-X.